Nuclear Science and Techniques (2025) 36:138
https://doi.org/10.1007/s41365-025-01720-5

Correlations of the net baryon number and electric charge in nuclear matter

Xin-Ran Yang[1,2] · Guo-Yun Shao[1,2] · Chong-Long Xie[1,2] · Zhi-Peng Li[1,2]

Received: 30 August 2024 / Revised: 28 December 2024 / Accepted: 7 January 2025 / Published online: 3 June 2025

Abstract
We investigated the correlations between the net baryon number and electric charge up to the sixth order related to the interactions of nuclear matter at low temperature and explored their relationship with the nuclear liquid–gas phase transition (LGPT) within the framework of the nonlinear Walecka model. The calculations showed that strong correlations between the baryon number and electric charge existed near the LGPT, and higher-order correlations were more sensitive than the lower-order correlations near the phase transition. However, in the high-temperature region away from the LGPT, the rescaled lower-order correlations were relatively larger than most of the higher-order correlations. In addition, some of the fifth- and sixth-order correlations possibly changed sign from negative to positive along the chemical freeze-out line with decreasing temperature. In combination with future experimental projects at lower collision energies, the derived results can be used to study the phase structure of strongly interacting matter and analyze the related experimental signals.

Keywords Correlations of conserved charges · Nuclear matter · Nuclear liquid–gas phase transition · Heavy-ion collision

1 Introduction

Mapping the phase diagram of quantum chromodynamics (QCD) is a primary objective in nuclear physics, which involves chiral and deconfinement phase transitions related to the transformation of quark-gluon plasma to hadronic matter [1]. The calculations from lattice QCD and hadron resonance gas (HRG) model indicate that a smooth crossover transformation occurs at high temperatures and small chemical potentials [2–8]. Furthermore, studies on effective quark models [9–23], the Dyson–Schwinger equation approach [24–29], the functional renormalization group theory [30–32], and machine learning [33] suggest that a first-order chiral phase transition occurs at large chemical potentials.

The fluctuations and correlations of conserved charges (baryon number B, electric charge Q, and strangeness S) are sensitive observables for studying the phase transitions of strongly interacting matter [34, 35]. The net proton (proxy for net baryon) cumulants measured in the beam energy scan (BES) program at the relativistic heavy-ion collider (RHIC) [36–42] has inspired extensive studies on QCD phase transition, particularly the QCD critical endpoint (CEP). More impressively, the distributions of the net proton number at the center-of-mass energy $\sqrt{s_{\rm NN}} = 3$ GeV and 2.4 GeV are different from those at 7.7 GeV and above because the fluctuation distributions of the net proton number are primarily dominated by the interaction among hadrons [40].

The experimental results at 3 GeV and below necessitate studies on the effect of hadronic interactions on the fluctuations of conserved charges at lower energies [43–46]. The nuclear liquid–gas phase transition (LGPT) may be involved at lower collision energies [47–63].

A van der Waals model was used to study the high-order distributions of the net baryon number in both pure

This work was supported by the National Natural Science Foundation of China (Nos. 12475145, 11875213), and the Natural Science Basic Research Plan in Shaanxi Province of China (No. 2024JC-YBMS-018).

✉ Guo-Yun Shao
gyshao@mail.xjtu.edu.cn

[1] School of Physics, Xi'an Jiaotong University, Xi'an 710049, China

[2] MOE Key Laboratory for Nonequilibrium Synthesis and Modulation of Condensed Matter, Xi'an Jiaotong University, Xi'an 710049, China

and mixed phases of the LGPT [64–66]. The second-order susceptibility of the net baryon number for positive- and negative-parity nucleons was examined near the chiral and nuclear liquid–gas phase transitions using a double-parity model, in which both the chiral phase transition and nuclear LGPT are effectively included [45]. The net baryon kurtosis and skewness were considered in the non-linear Walecka model to analyze the experimental signals at lower collision energies [55, 56]. The hyperskewness and hyperkurtosis of the net baryon number were recently calculated to explore the relationship between nuclear LGPT and experimental observables [67].

Because the interactions among hadrons dominate the density fluctuations in lower-energy regimes (below 3 GeV), the BES program at collision energies lower than 7.7 GeV is expected to provide detailed information on the phase structure of strongly interacting matter. Additionally, relevant experiments have been planned at the high intensity heavy-ion accelerator facility (HIAF). Meanwhile, the HADES collaboration at the GSI Helmholtzzentrum für Schwerionenforschung planned to measure the higher-order net proton and net charge fluctuations in the central Au + Au reactions at collision energies ranging from 0.2 A to 1.0 A GeV to probe the LGPT region [68]. These experiments are significant for investigating nuclear liquid–gas and chiral phase transitions through density fluctuations.

In addition to the fluctuations in conserved charges, the correlations between different conserved charges provide important information for exploring phase transitions. The correlations of conserved charges or off-diagonal susceptibilities have been calculated to study the chiral and deconfinement phase transitions at high temperatures in lattice QCD and some effective quark models (e.g., [69–75]). However, correlations between the net baryon number and electric charge in nuclear matter and their relationship with nuclear LGPT, which are useful for diagnosing the phase diagram of strongly interacting matter at low temperatures, have not yet been explored. In this study, we explored the correlations between the net baryon number and electric charge up to the sixth order in nuclear matter using the nonlinear Walecka model. The characteristic behaviors of correlations evoked by the nucleon–nucleon interaction, both near and far away from the nuclear LGPT, were obtained. These results are expected to aid future analyses of chiral phase transitions, nuclear LGPT, and related experimental signals.

The remainder of this paper is organized as follows. In Sect. 2, we introduce formulas to describe the correlations between conserved charges and the nonlinear Walecka model. In Sect. 3, we illustrate the numerical results for the correlation between the net baryon number and electric charge. Finally, a summary is presented in Sect. 4.

2 Theoretical descriptions

The fluctuations and correlations of conserved charges are related to the equation of state of a thermodynamic system. In the grand canonical ensemble of strongly interacting matter, the pressure is the logarithm of the partition function [76]:

$$P = \frac{T}{V} \ln Z(V, T, \mu_{\rm B}, \mu_{\rm Q}, \mu_{\rm S}), \tag{1}$$

where $\mu_{\rm B}$, $\mu_{\rm Q}$, $\mu_{\rm S}$ are the chemical potentials of the conserved charges, that is, the baryon number, electric charge, and strangeness in a strong interaction, respectively. The generalized susceptibilities are derived by taking the partial derivatives of the pressure with respect to the corresponding chemical potentials [39]

$$\chi^{\rm BQS}_{ijk} = \frac{\partial^{i+j+k}[P/T^4]}{\partial(\mu_{\rm B}/T)^i \partial(\mu_{\rm Q}/T)^j \partial(\mu_{\rm S}/T)^k}. \tag{2}$$

The cumulants of the multiplicity distributions of the conserved charges are usually measured experimentally. These are related to the generalized susceptibilities by

$$C^{\rm BQS}_{ijk} = \frac{\partial^{i+j+k} \ln[Z(V, T, \mu_{\rm B}, \mu_{\rm Q}, \mu_{\rm S})]}{\partial(\mu_{\rm B}/T)^i \partial(\mu_{\rm Q}/T)^j \partial(\mu_{\rm S}/T)^k} = VT^3 \chi^{\rm BQS}_{ijk}. \tag{3}$$

To eliminate the volume dependence in heavy-ion collision experiments, observables are usually constructed using the ratios of cumulants and then compared with the theoretical calculations of the generalized susceptibilities with

$$\frac{C^{\rm BQS}_{ijk}}{C^{\rm BQS}_{\rm lmn}} = \frac{\chi^{\rm BQS}_{ijk}}{\chi^{\rm BQS}_{\rm lmn}}. \tag{4}$$

In this study, the nonlinear Walecka model was used to calculate the correlations between the net baryon number and electric charge in nuclear matter at low temperatures. This model describes the properties of finite nuclei and the equation of state of nuclear matter. The approximate equivalence of this model with the HRG model at low temperatures and densities is also indicated in Ref. [77]. This model was recently used to explore fluctuations in the net baryon number in nuclear matter, for example, kurtosis and skewness [55, 56] and hyperskewness and hyperkurtosis [67].

The Lagrangian density for the nucleon-meson system in the nonlinear Walecka model [54, 78] is

$$\begin{aligned}\mathcal{L}=&\sum_N \bar{\psi}_N\left[i\gamma_\mu\partial^\mu-(m_N-g_\sigma\sigma)-g_\omega\gamma_\mu\omega^\mu-g_\rho\gamma_\mu\boldsymbol{\tau}\cdot\boldsymbol{\rho}^\mu\right]\psi_N\\&+\frac{1}{2}\left(\partial_\mu\sigma\partial^\mu\sigma-m_\sigma^2\sigma^2\right)-\frac{1}{3}bm_N\left(g_\sigma\sigma\right)^3-\frac{1}{4}c\left(g_\sigma\sigma\right)^4\\&+\frac{1}{2}m_\omega^2\omega_\mu\omega^\mu-\frac{1}{4}\omega_{\mu\nu}\omega^{\mu\nu}\\&+\frac{1}{2}m_\rho^2\boldsymbol{\rho}_\mu\cdot\boldsymbol{\rho}^\mu-\frac{1}{4}\boldsymbol{\rho}_{\mu\nu}\cdot\boldsymbol{\rho}^{\mu\nu},\end{aligned}\tag{5}$$

where $\omega_{\mu\nu}=\partial_\mu\omega_\nu-\partial_\nu\omega_\mu$, $\rho_{\mu\nu}=\partial_\mu\boldsymbol{\rho}_\nu-\partial_\nu\boldsymbol{\rho}_\mu$, and m_N are the nucleon mass in vacuum. The interactions between nucleons are mediated by σ, ω, ρ mesons.

The thermodynamic potential can be derived in the mean-field approximation as

$$\begin{aligned}\Omega=&-\beta^{-1}\sum_N 2\int\frac{d^3\boldsymbol{k}}{(2\pi)^3}\Big[\ln\Big(1+e^{-\beta\left(E_N^*(k)-\mu_N^*\right)}\Big)\\&+\ln\Big(1+e^{-\beta\left(E_N^*(k)+\mu_N^*\right)}\Big)\Big]+\frac{1}{2}m_\sigma^2\sigma^2+\frac{1}{3}bm_N\left(g_\sigma\sigma\right)^3\\&+\frac{1}{4}c\left(g_\sigma\sigma\right)^4-\frac{1}{2}m_\omega^2\omega^2-\frac{1}{2}m_\rho^2\rho_3^2,\end{aligned}\tag{6}$$

where $\beta=1/T$, $E_{\mathrm{N}}^*=\sqrt{k^2+m_{\mathrm{N}}^{*2}}$, and ρ_3 denote the third component of the ρ meson field. The effective nucleon mass $m_{\mathrm{N}}^*=m_{\mathrm{N}}-g_\sigma\sigma$ and effective chemical potential μ_{N}^* are defined as $\mu_{\mathrm{N}}^*=\mu_{\mathrm{N}}-g_\omega\omega-\tau_{3\,\mathrm{N}}g_\rho\rho_3$ ($\tau_{3\,\mathrm{N}}=1/2$ for proton, $-1/2$ for neutron).

Minimizing the thermodynamical potential

$$\frac{\partial\Omega}{\partial\sigma}=\frac{\partial\Omega}{\partial\omega}=\frac{\partial\Omega}{\partial\rho_3}=0,\tag{7}$$

the meson field equations can be derived as:

$$g_\sigma\sigma=\left(\frac{g_\sigma}{m_\sigma}\right)^2\left[\rho_{\mathrm{p}}^s+\rho_{\mathrm{n}}^s-bm_{\mathrm{N}}\left(g_\sigma\sigma\right)^2-c\left(g_\sigma\sigma\right)^3\right],\tag{8}$$

$$g_\omega\omega=\left(\frac{g_\omega}{m_\omega}\right)^2\left(\rho_{\mathrm{p}}+\rho_{\mathrm{n}}\right),\tag{9}$$

$$g_\rho\rho_3=\frac{1}{2}\left(\frac{g_\rho}{m_\rho}\right)^2\left(\rho_{\mathrm{p}}-\rho_{\mathrm{n}}\right).\tag{10}$$

In Eqs.(8)–(10), the nucleon number density

$$\rho_i=2\int\frac{\mathrm{d}^3\boldsymbol{k}}{(2\pi)^3}[f\left(E_i^*-\mu_i^*\right)-\bar{f}\left(E_i^*+\mu_i^*\right)],\tag{11}$$

and scalar density

$$\rho_i^{\mathrm{s}}=2\int\frac{\mathrm{d}^3\boldsymbol{k}}{(2\pi)^3}\frac{m_i^*}{E_i^*}[f\left(E_i^*-\mu_i^*\right)+\bar{f}\left(E_i^*+\mu_i^*\right)],\tag{12}$$

where $f(E_i^*-\mu_i^*)$ and $\bar{f}(E_i^*+\mu_i^*)$ are the fermion and antifermion distribution functions, respectively, with

$$f(E_i^*-\mu_i^*)=\frac{1}{1+\exp\left\{\left[E_i^*-\mu_i^*\right]/T\right\}},\tag{13}$$

and

$$f(E_i^*+\mu_i^*)=\frac{1}{1+\exp\left\{\left[E_i^*+\mu_i^*\right]/T\right\}}.\tag{14}$$

The meson field equations can be solved for a given temperature and chemical potential (or baryon number density). The model parameters, g_σ, g_ω, g_ρ, b and c, are listed in Table 1. They were fitted with the compression modulus $K=240$ MeV, symmetric energy $a_{\mathrm{sym}}=31.3$ MeV, effective nucleon mass $m_{\mathrm{N}}^*=m_{\mathrm{N}}-g_\sigma\sigma=0.75\,m_{\mathrm{N}}$, and binding energy $B/A=-16.0$ MeV at nuclear saturation density with $\rho_0=0.16\,\mathrm{fm}^{-3}$.

3 Results and discussion

In this section, we present the numerical results for the correlation between the net baryon number and electric charge in the nonlinear Walecka model. To simulate the physical conditions in the BES program at RHIC STAR, the isospin asymmetric nuclear matter was considered in the calculation with the constraint $\rho_{\mathrm{Q}}/\rho_{\mathrm{B}}=0.4$. In the present Walecka model, strange baryons were not included; thus, the strangeness condition $\rho_{\mathrm{S}}=0$ was automatically satisfied. $\rho_{\mathrm{Q}}/\rho_{\mathrm{B}}=0.4$ might deviate slightly owing to isospin dynamics. The influence of different isospin asymmetries on the fluctuations and correlations of conserved charges will be explored in detail in a separate study.

The correlations between the baryon number and electric charge are related to the baryon (μ_{B}) and isospin μ_{Q} ($\mu_{\mathrm{Q}}=\mu_{\mathrm{p}}-\mu_{\mathrm{n}}$) chemical potentials. In Fig. 1, we demonstrate the value of μ_{Q} as a function of the temperature and baryon chemical potential by first plotting the contour map of μ_{Q} in the $T-\mu_{\mathrm{B}}$ plane derived under the constraint of $\rho_{\mathrm{Q}}/\rho_{\mathrm{B}}=0.4$. Additionally, the corresponding liquid–gas phase transition line with a CEP located at $T=13$ MeV and

Table 1 Parameters in the nonlinear Walecka model

$(g_\sigma/m_\sigma)^2$ (fm^2)	$(g_\omega/m_\omega)^2$ (fm^2)	$(g_\rho/m_\rho)^2$ (fm^2)	b	c
10.329	5.423	0.95	0.00692	−0.0048

$\mu_B = 919$ MeV is plotted in this figure. To compare with the chiral crossover phase transition of quarks, the dashed "Line A" in Fig. 1 was derived under the condition that the value of $\partial\sigma/\partial\mu_B$ was maximum for each given temperature. To a certain degree, this line is analogous to a chiral crossover transformation, although it is not a true phase transition in nuclear matter. It indicates the location at which the dynamic nucleon mass changes most rapidly with an increase in the chemical potential. The reason for plotting "Line A" is to emphasize that both the σ field in nuclear matter and the quark condensate in quark matter are associated with the dynamic mass of fermions, and therefore, the rapid change of mass might have a universal effect on the fluctuation distributions of conserved charges. As indicated in our previous studies [54, 55, 67], the location of line A helps us understand the behavior of the interaction measurement (trace anomaly) and the fluctuations of conserved charges near the phase transition [55, 67].

Additionally, "Line A" can be defined by the maximum point of $\partial\omega/\partial\mu_B$ or $\partial n_B/\partial\mu_B$, because the density can be considered as the order parameter for liquid–gas phase transition. Under this definition, the results obtained using the quark model do not correspond to a chiral crossover phase transition. However, this was not the purpose of the present study. Our aim was to identify common properties related to the dynamical fermion mass near the critical region of a first-order phase transition. However, the calculation indicates that the curves ("Line A") under the two definitions coincide near the critical region and gradually deviate at higher temperatures away from the critical region.

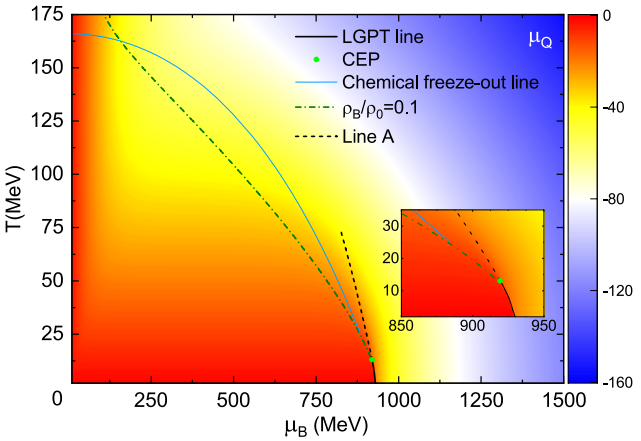

Fig. 1 (Color online) Contour of μ_Q in the $T-\mu_B$ plane derived in the nonlinear Walecka model with the constraint of $\rho_Q/\rho_B = 0.4$. The solid line is the liquid–gas transition line with a CEP located at $T = 13$ MeV and $\mu_B = 919$ MeV. The blue line is the chemical freeze-out line fitted in Ref. [79]. The dash-dotted line corresponds to the temperature and chemical potential for $\rho_B = 0.1\rho_0$. "Line A" is derived using the maximum value of $\partial\sigma/\partial\mu_B$ for each given temperature

For convenience, in the subsequent discussion of the experimental observables, we include a plot of the chemical freeze-out line fitted to the experimental data at high energies in Fig. 1 [79], which can be described by

$$T(\mu_B) = a - b\mu_B^2 - c\mu_B^4, \tag{15}$$

where $a = 0.166\,\text{GeV}$, $b = 0.139\,\text{GeV}^{-1}$ and $c = 0.053\,\text{GeV}^{-3}$.

It should be noted that the trajectories of the present relativistic heavy-ion collisions do not pass through T_C of nuclear LGPT. It is still not known how far the realistic chemical freeze-out line is from the critical region at the present time. However, similar to the chiral phase transition of quarks, the existence of nuclear LGPT affects the fluctuation and correlation of the net baryon and electric charge numbers in the region not adjacent to the critical endpoint in intermediate-energy heavy-ion collision experiments. The numerical results for the parameterized chemical freeze-out line in this study can be used as a reference. The realistic chemical freeze-out conditions at intermediate and low energies will be extracted in future heavy-ion collision experiments. The contribution from LGPT needs to be considered when analyzing the experimental data.

Figure 1 shows that the value of $|\mu_Q|$ is less than 40 MeV in the red area. In this region, the baryon number density is very small, which is approximately indicated by the temperature and chemical potential curves for $\rho_B = 0.1\rho_0$ (dash-dotted line). The value of $|\mu_Q|$ increases with the baryon density (corresponding to a larger chemical potential). This trend in $|\mu_Q|$ is illustrated in Fig. 1. Along the chemical freeze-out line (solid blue line), changes in μ_Q during freeze-out with decreasing temperature or collision energy are observed.

Figure 2 shows the second-order correlation between the baryon number and electric charge, χ_{11}^{BQ}/χ_2^Q, as a function of the baryon chemical potential for $T = 75, 50, 25$ MeV. To derive a physical quantity comparable with future experimental data, the correlated susceptibility was divided by χ_2^Q to eliminates volume dependence. For each temperature, the rescaled second-order correlation χ_{11}^{BQ}/χ_2^Q shown in Fig. 2 displays nonmonotonic behavior with a peak at a certain chemical potential. The values of these peaks increase with decreasing temperature, which indicates that the correlation between the baryon number and electric charge is enhanced near the phase transition region. The solid dots in Fig. 2 show the values for the chemical freeze-out described by Eq. (15), which illustrates that the value of χ_{11}^{BQ}/χ_2^Q increases along the freeze-out line when moving from the high-temperature region to the critical region.

Figure 3 shows the third-order correlations χ_{12}^{BQ}/χ_2^Q and χ_{21}^{BQ}/χ_2^Q as functions of the chemical potential at several

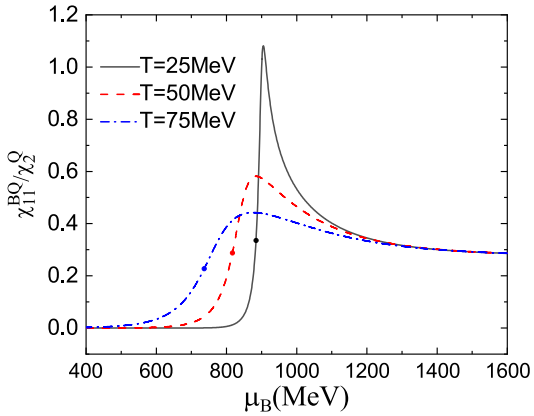

Fig. 2 (Color online) Second-order correlation between the baryon number and electric charge as a function of the chemical potential for different temperatures. The solid dots indicate the values on the chemical freeze-out line given in Fig. 1

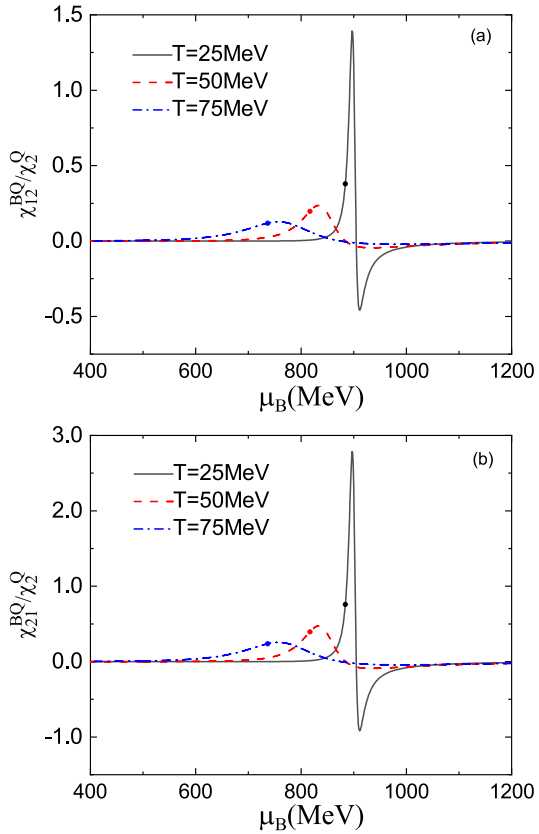

Fig. 3 (Color online) Third-order correlations between the baryon number and electric charge as functions of the chemical potential at different temperatures. The solid dots indicate the values on the chemical freeze-out line plotted in Fig. 1

temperatures. Compared with χ_{12}^{BQ}/χ_2^Q, χ_{21}^{BQ}/χ_2^Q exhibits relatively larger fluctuations at the same temperature. The solid dots on the chemical freeze-out line show the same trend. This means that the measurement of χ_{21}^{BQ}/χ_2^Q is more sensitive than χ_{12}^{BQ}/χ_2^Q in heavy-ion collision experiments. Figure 3 also indicates that the correlations between the baryon number and electric charge intensify with decreasing temperatures. Evident oscillations of χ_{12}^{BQ}/χ_2^Q and χ_{21}^{BQ}/χ_2^Q appear for $T = 25$ MeV, accompanied by alternating positives and negatives. As the temperature decreases, divergent behavior occurs at the CEP of LGPT. These features can be used to determine the signal for the phase transition in the experiments.

In Fig. 4, we plot the fourth-order correlations between the baryon number and electric charge: χ_{13}^{BQ}/χ_2^Q, χ_{22}^{BQ}/χ_2^Q, and χ_{31}^{BQ}/χ_2^Q. Compared to the second- and third-order correlations, Figs. 2, 3, and 4 show that the fourth-order correlations rescaled by χ_2^Q are weaker at higher temperatures such as $T = 75$ MeV. However, the correlations are much stronger at $T = 25$ MeV, near the critical region of LGPT. Correspondingly, with an increase in the chemical potential at lower temperatures, a bimodal structure evidently exists for all three correlations. In addition, the maximum values of χ_{13}^{BQ}/χ_2^Q, χ_{22}^{BQ}/χ_2^Q, and χ_{31}^{BQ}/χ_2^Q increase sequentially. Furthermore, the solid dots demonstrate that the value of each correlation during freeze-out increases with the decreasing temperatures. Moreover, $\chi_{13}^{BQ}/\chi_2^Q < \chi_{22}^{BQ}/\chi_2^Q < \chi_{31}^{BQ}/\chi_2^Q$ during chemical freeze-out at each temperature, which implies that χ_{31}^{BQ}/χ_2^Q is the most sensitive among the three fourth-order correlations.

Figure 5 presents the fifth-order correlations between the baryon number and electric charge, χ_{14}^{BQ}/χ_2^Q, χ_{23}^{BQ}/χ_2^Q, χ_{32}^{BQ}/χ_2^Q, and χ_{41}^{BQ}/χ_2^Q for $T = 75, 50, 25$ MeV. At $T = 75$ MeV, the values of the four rescaled correlations are small; however, they become significant at $T = 25$ MeV. Combined with the phase diagrams shown in Fig. 1, it is seen that the high-order correlated fluctuations strengthen as they approach the liquid–gas transition. Similar to the fourth-order correlations, the rescaled fifth correlations fulfill the relationships $\left|\chi_{14}^{BQ}/\chi_2^Q\right| < \left|\chi_{23}^{BQ}/\chi_2^Q\right| < \left|\chi_{32}^{BQ}/\chi_2^Q\right| < \left|\chi_{41}^{BQ}/\chi_2^Q\right|$ at chemical freeze-out. Moreover, all the four fifth-order correlation fluctuations are negative at chemical freeze-out for $T = 75$ and 50 MeV; however, they are positive at $T = 25$ MeV, near the liquid–gas transition. This is a prominent feature for exploring the interactions and phase transitions of nuclear matter.

Figure 6 shows the sixth-order correlations of the baryon number and electric charge, that is, χ_{15}^{BQ}/χ_2^Q, χ_{24}^{BQ}/χ_2^Q, χ_{33}^{BQ}/χ_2^Q, χ_{42}^{BQ}/χ_2^Q, and χ_{51}^{BQ}/χ_2^Q. Each sixth-order correlation exhibits a double peak and double valley

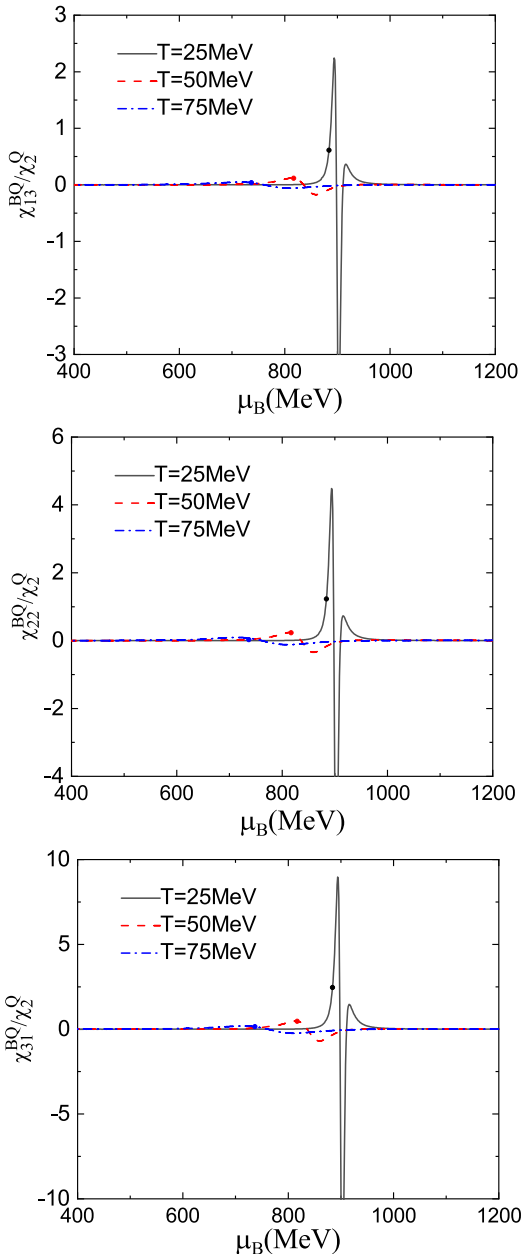

Fig. 4 (Color online) Fourth-order correlations between the baryon number and electric charge as functions of the chemical potential for different temperatures. The solid dots indicate the values on the chemical freeze-out line given in Fig. 1

structure, although one of the two peaks is not prominent. The oscillating behavior intensifies when moving toward the phase transition region from high to low temperatures. Similarly, the intensity of the oscillations increases from χ_{15}^{BQ}/χ_2^Q, χ_{24}^{BQ}/χ_2^Q, χ_{33}^{BQ}/χ_2^Q, χ_{42}^{BQ}/χ_2^Q to χ_{51}^{BQ}/χ_2^Q.

For a given order of correlations, the numerical results shown in Figs. 2, 3, 4, 5, and 6 indicate that the signals become stronger when taking the higher-order partial derivatives of the baryon chemical potential. Additionally, we examined the pure baryon number fluctuation and found that its highest sensitivity was of the same order as the LGPT critical endpoint, possibly because the baryon number fluctuation includes both proton and neutron contributions. However, the electric charge fluctuation involves the isospin density $\rho_N - \rho_P$. The baryon number density is always larger than the isospin density, which is associated with stronger fluctuations when there are more derivatives with respect to the baryon chemical potential than that with to electric chemical potential for a given order of correlations.

In addition, a comparison of the results shown in Fig. 2, 3, 4, 5, and 6 shows that the rescaled higher-order correlations fluctuate more strongly near the phase transition region, whereas the lower-order correlations at high temperatures are larger than most of the higher-order correlations away from the phase transition region. A similar phenomenon occurs in the correlations of conserved charges in quark matter [74]. According to the fluctuations of net baryon number [55, 67] and the correlations between net baryon number and electric charge in this study, the fluctuations and correlations of conserved charges have similar organizational structures for nuclear and quark matter. This is primarily attributed to the fact that the two phase transitions belong to the same universal class, and both describe the interaction of matter with temperature- and chemical potential-dependent fermion masses.

Because the QCD phase transition and nuclear LGPT possibly occur sequentially from high to low temperatures (even if LGPT is not triggered), the energy-dependent behaviors of the fluctuations and correlations can be referenced to determine the phase transition signals of the strongly interacting matter. Although the latest reported BES II high-precision data at 7.7 – 39 GeV do not display a drastic change in the net baryon number kurtosis, stronger fluctuation signals may appear in heavy-ion experiments with collision energies lower than 7.7 GeV. Furthermore, in the hadronic interaction dominant evolution with collision energies lower than the threshold of the generation of QGP, the nuclear interaction and phase structure of LGPT will dominate over the behavior of fluctuations and correlations of conserved charges. The nature of the changes in fluctuations and correlations with decreasing collision energy during experiments requires investigation.

4 Summary

Fluctuations and correlations between conserved charges are sensitive probes for investigating the phase structure of strongly interacting matter. In this study, we used the nonlinear Walecka model to calculate the correlations

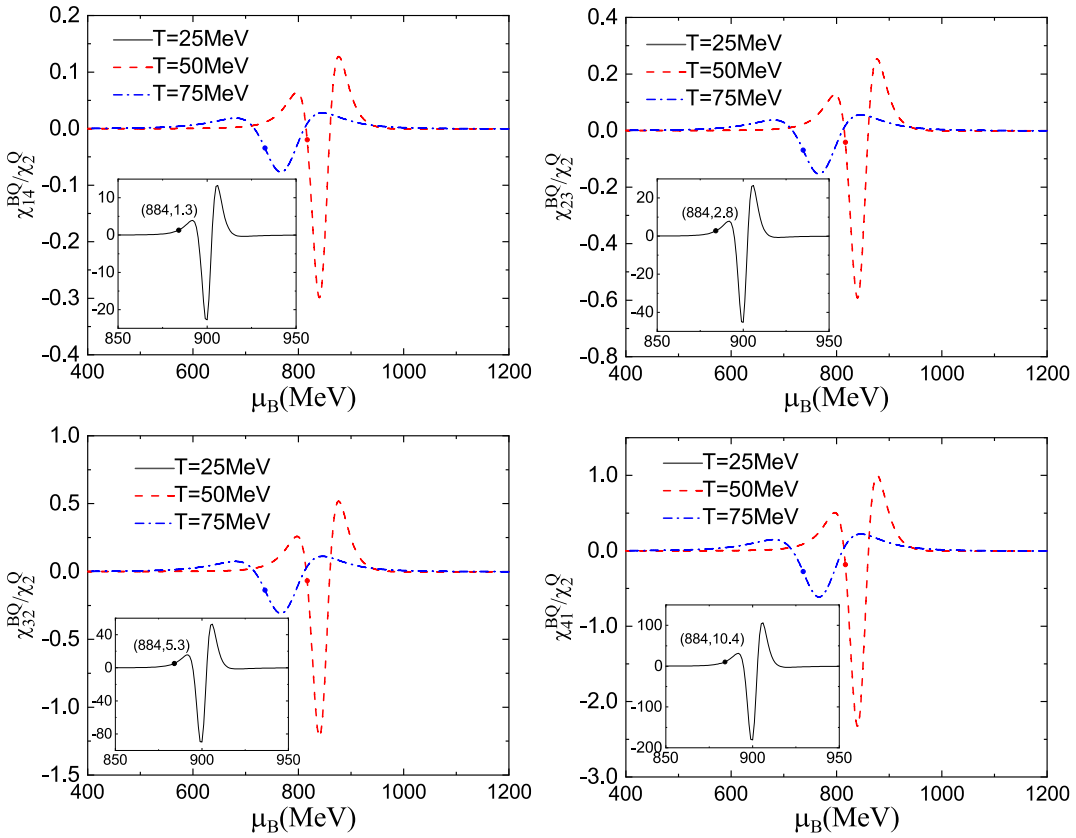

Fig. 5 (Color online) Fifth-order correlations between the baryon number and electric charge as functions of the chemical potential for different temperatures. The solid dots indicate the values on the chemical freeze-out line given in Fig. 1

between the net baryon number and electric charge up to the sixth order, which originated from hadronic interactions in nuclear matter and explored their relationship with the nuclear liquid–gas phase transition.

The calculation indicated that the correlations between the net baryon number and electric charge gradually became stronger from the high-temperature region to the critical region of the nuclear LGPT. In particular, the correlations were significant at the location where the σ field or nucleon mass changed rapidly near the critical region. Similar behavior was observed for the chiral crossover phase transition of quark matter, primarily because of the similar dynamic mass evolution and same universal class of the chiral phase transition of quark matter and the liquid–gas phase transition of nuclear matter.

Compared to the lower-order correlations, the higher-order correlations fluctuated more strongly near the phase transition region, whereas the rescaled lower-order correlations were relatively stronger than most of the higher-order correlations away from the phase transition region at high temperatures. At the chemical freeze-out for each temperature, the calculation indicated that $\chi_{13}^{BQ}/\chi_2^Q < \chi_{22}^{BQ}/\chi_2^Q < \chi_{31}^{BQ}/\chi_2^Q$ for the fourth-order correlation, $|\chi_{14}^{BQ}/\chi_2^Q| < |\chi_{23}^{BQ}/\chi_2^Q| < |\chi_{32}^{BQ}/\chi_2^Q| < |\chi_{41}^{BQ}/\chi_2^Q|$ for the fifth-order correlations, and $|\chi_{15}^{BQ}/\chi_2^Q| < |\chi_{24}^{BQ}/\chi_2^Q| < |\chi_{33}^{BQ}/\chi_2^Q| < |\chi_{42}^{BQ}/\chi_2^Q| < |\chi_{51}^{BQ}/\chi_2^Q|$ for the sixth-order correlations. In particular, the values of the fifth- and sixth-order correlations changed from negative to positive when approaching the critical region of LGPT from the high-temperature side along the extrapolated chemical freeze-out line. With the availability of more precise data from experiments below 7.7 GeV in the future, realistic chemical freeze-out conditions can be fitted, and the results obtained in this study can be used to analyze the signals

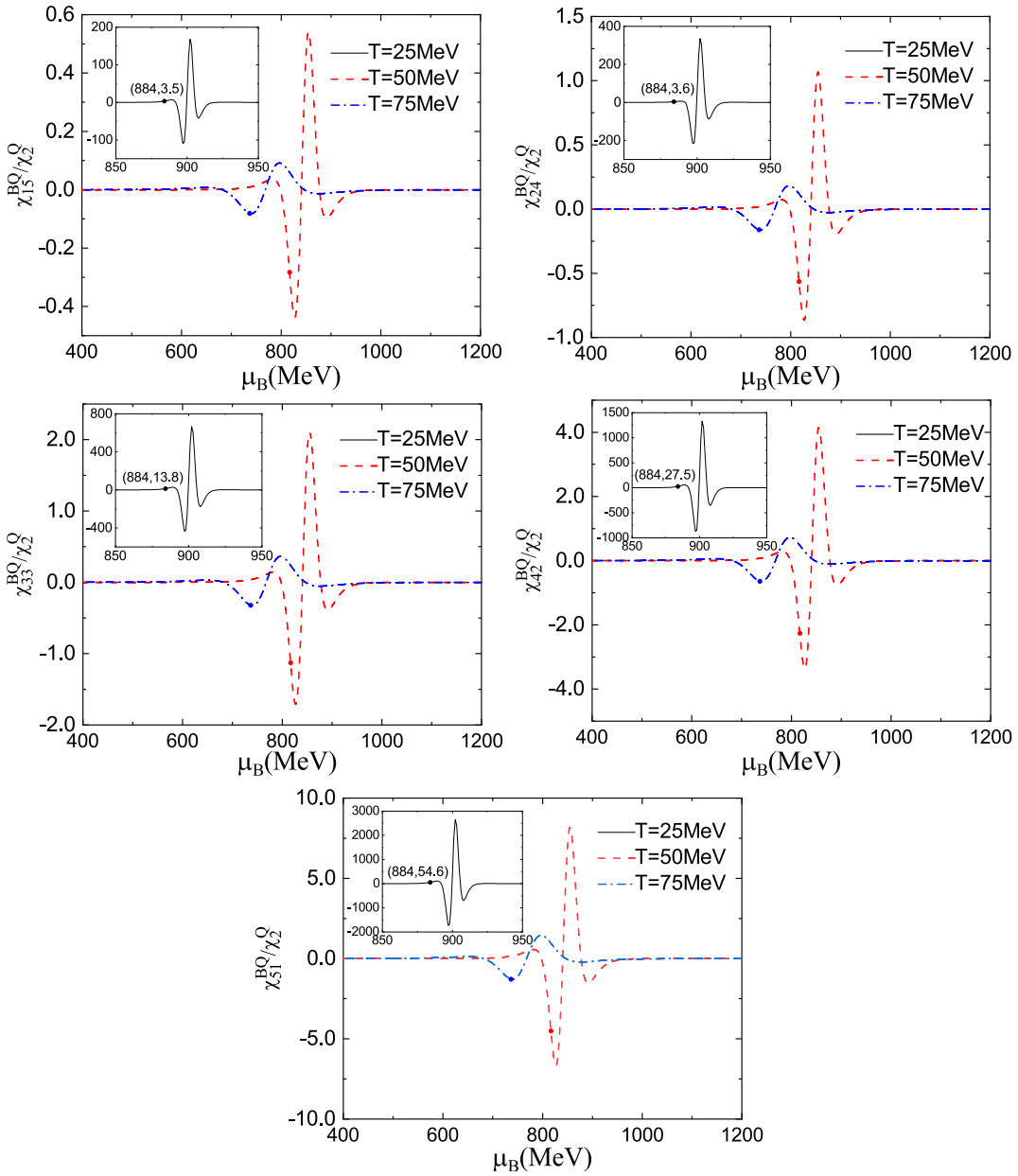

Fig. 6 (Color online) Sixth-order correlations between the baryon number and electric charge as functions of the chemical potential for different temperatures. The solid dots demonstrate the values on the chemical freeze-out line given in Fig. 1

of QCD phase transitions and the influence of the nuclear liquid–gas phase transition.

Author contributions All authors contributed to the study conception and design. Material preparation, data collection, and analysis were performed by Xin-Ran Yang, Guo-Yun Shao, Chong-Long Xie, and Zhi-Peng Li. The first draft of the manuscript was written by Guo-Yun Shao, and all authors commented on previous versions of the manuscript. All authors read and approved the final manuscript.

Data availability The data that support the findings of this study are openly available in Science Data Bank at https://cstr.cn/31253.11.sciencedb.j00186.00224 and https://doi.org/10.57760/sciencedb.j00186.00224.

Declarations

Conflict of interest The authors declare that they have no conflict of interest.

References

1. Q.Y. Shou, Y.G. Ma, S. Zhang et al., Properties of QCD matter: a review of selected results from ALICE experiment. Nucl. Sci. Tech. **35**, 219 (2024). https://doi.org/10.1007/s41365-024-01583-2
2. Y. Aoki, G. Endrodi, Z. Fodor et al., The order of the quantum chromodynamics transition predicted by the standard model of particle physics. Nature **443**, 675–678 (2006). https://doi.org/10.1038/nature05120
3. A. Bazavov, H.T. Ding, P. Hegde et al., (HotQCD Collaboration), Chiral crossover in QCD at zero and non-zero chemical potentials. Phys. Lett. B **795**, 15 (2019). https://doi.org/10.1016/j.physletb.2019.05.013
4. S. Borsányi, Z. Fodor, S.D. Katz et al., Freeze-out parameters: lattice meets experiment. Phys. Rev. Lett. **111**, 062005 (2013). https://doi.org/10.1103/PhysRevLett.111.062005
5. A. Bazavov, T. Bhattacharya, C. DeTar et al., (HotQCD Collaboration), equation of state in (2+1)-flavor QCD. Phys. Rev. D **90**, 094503 (2014). https://doi.org/10.1103/PhysRevD.90.094503
6. A. Bazavov, H.T. Ding, P. Hegde et al., (HotQCD Collaboration), Skewness and kurtosis of net baryon-number distributions at small values of the baryon chemical potential. Phys. Rev. D **96**, 074510 (2017). https://doi.org/10.1103/PhysRevD.96.074510
7. S. Borsányi, Z. Fodor, C. Hoelbling et al., Full result for the QCD equation of state with flavors. Phys. Lett. B **730**, 99 (2014). https://doi.org/10.1016/j.physletb.2014.01.007
8. S. Borsányi, Z. Fodor, J.N. Guenther et al., QCD Crossover at finite chemical potential from lattice simulations. Phys. Rev. Lett. **125**, 052001 (2020). https://doi.org/10.1103/PhysRevLett.125.052001
9. K. Fukushima, Chiral effective model with the Polyakov loop. Phys. Lett. B **591**, 277 (2004). https://doi.org/10.1016/j.physletb.2004.04.027
10. C. Ratti, M.A. Thaler, W. Weise, Phases of QCD: lattice thermodynamics and a field theoretical model. Phys. Rev. D **73**, 014019 (2006). https://doi.org/10.1103/PhysRevD.73.014019
11. P. Costa, M.C. Ruivo, C.A. De Sousa et al., Phase diagram and critical properties within an effective model of QCD: the Nambu-Jona-Lasinio model coupled to the Polyakov loop. Symmetry **2**, 1338–1374 (2010). https://doi.org/10.3390/sym2031338
12. W.J. Fu, Z. Zhang, Y.X. Liu, 2+1 flavor Polyakov-Nambu-Jona-Lasinio model at finite temperature and nonzero chemical potential. Phys. Rev. D **77**, 014006 (2008). https://doi.org/10.1103/PhysRevD.77.014006
13. T. Sasaki, J. Takahashi, Y. Sakai et al., Theta vacuum and entanglement interaction in the three-flavor Polyakov-loop extended Nambu-Jona-Lasinio model. Phys. Rev. D **85**, 056009 (2012). https://doi.org/10.1103/PhysRevD.85.056009
14. M. Ferreira, P. Costa, C. Providência, Deconfinement, chiral symmetry restoration and thermodynamics of (2+1)-flavor hot QCD matter in an external magnetic field. Phys. Rev. D **89**, 036006 (2014). https://doi.org/10.1103/PhysRevD.89.036006
15. Y.Q. Zhao, S. He, D.F. Hou et al., Phase diagram of holographic thermal dense QCD matter with rotation. J. High Energy Phys. **04**, 115 (2023). https://doi.org/10.1007/JHEP04(2023)115
16. G.Y. Shao, Z.D. Tang, X.Y. Gao et al., Baryon number fluctuations and the phase structure in the PNJL model. Eur. Phys. J. C **78**, 138 (2018). https://doi.org/10.1140/epjc/s10052-018-5636-0
17. B.J. Schaefer, M. Wagner, J. Wambach, Thermodynamics of (2+1)-flavor QCD: confronting models with lattice studies. Phys. Rev. D **81**, 074013 (2010). https://doi.org/10.1103/PhysRevD.81.074013
18. V. Skokov, B. Friman, K. Redlich, Quark number fluctuations in the Polyakov loop-extended quark-meson model at finite baryon density. Phys. Rev. C **83**, 054904 (2011). https://doi.org/10.1103/PhysRevC.83.054904
19. L.M. Liu, J. Xu, G.X. Peng, Three-dimensional QCD phase diagram with a pion condensate in the NJL model. Phys. Rev. D **104**, 076009 (2021). https://doi.org/10.1103/PhysRevD.104.076009
20. X. Chen, D.N. Li, D.F. Hou et al., Quarkyonic phase from quenched dynamical holographic QCD model. J. High Energy Phys. **2020**, 73 (2020). https://doi.org/10.1007/JHEP03(2020)073
21. M. Ferreira, P. Costa, C. Providência, Presence of a critical endpoint in the QCD phase diagram from the net-baryon number fluctuations. Phys. Rev. D **98**, 034006 (2018). https://doi.org/10.1103/PhysRevD.98.034006
22. Y.H. Yang, L. He, P.C. Chu, Properties of the phase diagram from the Nambu-Jona-Lasino model with a scalar-vector interaction. Nucl. Sci. Tech. **35**, 166 (2024). https://doi.org/10.1007/s41365-024-01559-2
23. Y.D. Chen, D.N. Li, M. Huang, Inhomogeneous chiral condensation under rotation in the holographic QCD. Phys. Rev. D **106**, 106002 (2022). https://doi.org/10.1103/PhysRevD.106.106002
24. F. Gao, Y.X. Liu, QCD phase transitions using the QCD Dyson-Schwinger equation approach. Nucl. Tech. (in Chinese) **46**, 040015 (2024). https://doi.org/10.11889/j.0253-3219.2023.hjs.46.040015
25. S.X. Qin, L. Chang, H. Chen et al., Phase diagram and critical end point for strongly interacting quarks. Phys. Rev. Lett. **106**, 172301 (2011). https://doi.org/10.1103/PhysRevLett.106.172301
26. F. Gao, J. Chen, Y.X. Liu et al., Phase diagram and thermal properties of strong-interaction matter. Phys. Rev. D **93**, 094019 (2016). https://doi.org/10.1103/PhysRevD.93.094019
27. F. Gao, J.M. Pawlowski, QCD phase structure from functional methods. Phys. Rev. D **102**, 034027 (2020). https://doi.org/10.1103/PhysRevD.102.034027
28. C.S. Fischer, J. Luecker, C.A. Welzbacher, Phase structure of three and four flavor QCD. Phys. Rev. D **90**, 034022 (2014). https://doi.org/10.1103/PhysRevD.90.034022
29. C. Shi, Y.L. Wang, Y. Jiang et al., Locate QCD critical end point in a continuum model study. J. High Energy Phys. **1407**, 014 (2014). https://doi.org/10.1007/JHEP07(2014)014
30. W.J. Fu, J.M. Pawlowski, F. Rennecke, QCD phase structure at finite temperature and density. Phys. Rev. D **101**, 054032 (2020). https://doi.org/10.1103/PhysRevD.101.054032
31. F. Rennecke, B.J. Schaefer, Fluctuation-induced modifications of the phase structure in (2+1)-flavor QCD. Phys. Rev. D **96**, 016009 (2017). https://doi.org/10.1103/PhysRevD.96.016009
32. W.J. Fu, X.F. Luo, J.M. Pawlowski et al., Hyper-order baryon number fluctuations at finite temperature and density. Phys. Rev. D **104**, 094047 (2021). https://doi.org/10.1103/PhysRevD.104.094047
33. Y.G. Ma, L.G. Pang, R. Wang et al., Phase transition study meets machine learning. Chin. Phys. Lett. **40**, 122101 (2023). https://doi.org/10.1088/0256-307X/40/12/122101
34. M.A. Stephanov, Non-Gaussian fluctuations near the QCD critical point. Phys. Rev. Lett. **102**, 032301 (2009). https://doi.org/10.1103/PhysRevLett.102.032301

35. M.A. Stephanov, Sign of Kurtosis near the QCD critical point. Phys. Rev. Lett. **107**, 052301 (2011). https://doi.org/10.1103/PhysRevLett.107.052301
36. M.M. Aggarwal, Z. Ahammed, A.V. Alakhverdyants et al., (STAR Collaboration), higher moments of net proton multiplicity distributions at RHIC. Phys. Rev. Lett. **105**, 022302 (2010). https://doi.org/10.1103/PhysRevLett.105.022302
37. L. Adamczyk, J.K. Adkins, G. Agakishiev et al., (STAR Collaboration), energy dependence of moments of net-proton multiplicity distributions at RHIC. Phys. Rev. Lett. **112**, 032302 (2014). https://doi.org/10.1103/PhysRevLett.112.032302
38. J.H. Chen, X.H. Dong, Properties of QCD matter: review of selected results from the relativistic heavy ion collider beam energy scan (RHIC BES) program. Nucl. Sci. Tech. **35**, 214 (2024). https://doi.org/10.1007/s41365-024-01591-2
39. X.F. Luo, N. Xu, Search for the QCD critical point with fluctuations of conserved quantities in relativistic heavy-ion collisions at RHIC: an overview. Nucl. Sci. Tech. **28**, 112 (2017). https://doi.org/10.1007/s41365-017-0257-0
40. B.E. Aboona, J. Adam, L. Adamczyk et al., (STAR Collaboration), measurement of sequential γ suppression in Au+Au collisions at $\sqrt{s_{NN}} = 200$GeV with the STAR experiment. Phys. Rev. Lett. **130**, 082301 (2023). https://doi.org/10.1103/PhysRevLett.130.112301
41. Y. Zhang, D.W. Zhang, X.F. Luo, Experimental study of the QCD phase diagram in relativistic heavy-ion collisions. Nucl. Tech. (in Chinese) **46**, 040001 (2024). https://doi.org/10.11889/j.0253-3219.2023.hjs.46.040001
42. Q. Chen, G.L. Ma, J.H. Chen, Transport model study of conserved charge fluctuations and QCD phase transition in heavy-ion collisions. Nucl. Tech. (In Chinese) **46**, 040013 (2023). https://doi.org/10.11889/j.0253-3219.2023.hjs.46.040013
43. C. Huang, Y.Y. Tan, R. Wen et al., Reconstruction of baryon number distributions. Chin. Phys. C **47**, 104106 (2023). https://doi.org/10.1088/1674-1137/aceee1
44. J.X. Shao, W.J. Fu, Y.X. Liu, Chemical freeze-out parameters via a functional renormalization group approach. Phys. Rev. D **109**, 034019 (2024). https://doi.org/10.1103/PhysRevD.109.034019
45. M. Marczenko, K. Redlich, C. Sasaki, Fluctuations near the liquid-gas and chiral phase transitions in hadronic matter. Phys. Rev. D **107**, 054046 (2023). https://doi.org/10.1103/PhysRevD.107.054046
46. C. Liu, X.G. Deng, Y.G. Ma, Density fluctuations in intermediate-energy heavy-ion collisions. Nucl. Sci. Tech. **33**, 52 (2022). https://doi.org/10.1007/s41365-022-01040-y
47. P. Chomaz, M. Colonna, J. Randrup, Nuclear spinodal fragmentation. Phys. Rep. **389**, 263 (2004). https://doi.org/10.1016/j.physrep.2003.09.006
48. J. Pochodzalla, T. Mohlenkamp, T. Rubehn et al., (ALADIN Collaboration), probing the nuclear liquid-gas phase transition. Phys. Rev. Lett. **75**, 1040 (1995). https://doi.org/10.1103/PhysRevLett.75.1040
49. B. Borderie, G. Tabacaru, P. Chomaz et al., (NDRA Collaboration), evidence for spinodal decomposition in nuclear multifragmentation. Phys. Rev. Lett. **86**, 3252 (2001). https://doi.org/10.1103/PhysRevLett.86.3252
50. A.S. Botvina, I.N. Mishustin, M. Begemann-Blaich et al., Multifragmentation of spectators in relativistic heavy-ion reactions. Nucl. Phys. A **584**, 737–756 (1995). https://doi.org/10.1016/0375-9474(94)00621-S
51. M. D'Agostino, A.S. Botvina, M. Bruno et al., Thermodynamical features of multifragmentation in peripheral Au + Au collisions at 35*A*MeV. Nucl. Phys. A **650**, 329–357 (1999). https://doi.org/10.1016/S0375-9474(99)00097-4
52. B.K. Srivastava, R.P. Scharenberg, S. Albergo et al., (EOS Collaboration), multifragmentation and the phase transition: a systematic study of the multifragmentation of 1*A*GeV Au, La, and Kr. Phys. Rev. C **65**, 054617 (2002). https://doi.org/10.1103/PhysRevC.65.054617
53. J.B. Elliott, L.G. Moretto, L. Phair et al., (ISiS Collaboration), liquid to vapor phase transition in excited nuclei. Phys. Rev. Lett. **88**, 042701 (2002). https://doi.org/10.1103/PhysRevLett.88.042701
54. W.B. He, G.Y. Shao, C.L. Xie, Speed of sound and liquid-gas phase transition in nuclear matter. Phys. Rev. C **107**, 014903 (2023). https://doi.org/10.1103/PhysRevC.107.014903
55. G.Y. Shao, X.Y. Gao, W.B. He, Baryon number fluctuations induced by hadronic interactions at low temperature and large chemical potential. Phys. Rev. D **101**, 074029 (2020). https://doi.org/10.1103/PhysRevD.101.074029
56. K. Xu, M. Huang, The baryon number fluctuation $\kappa\sigma^2$ as a probe of nuclear matter phase transition at high baryon density. arXiv:2307.12600v1. https://doi.org/10.48550/arXiv.2307.12600
57. Y.G. Ma, Application of information theory in nuclear liquid gas phase transition. Phys. Rev. Lett. **83**, 3617 (1999). https://doi.org/10.1103/PhysRevLett.83.3617
58. X.G. Deng, P. Danielewicz, Y.G. Ma et al., Impact of fragment formation on shear viscosity in the nuclear liquid-gas phase transition region. Phys. Rev. C **105**, 064613 (2022). https://doi.org/10.1103/PhysRevC.105.064613
59. M. Hempel, V. Dexheimer, S. Schramm et al., Noncongruence of the nuclear liquid-gas and deconfinement phase transitions. Phys. Rev. C **88**, 014906 (2013). https://doi.org/10.1103/PhysRevC.88.014906
60. A. Mukherjee, J. Steinheimer, S. Schramm, Higher-order baryon number susceptibilities: interplay between the chiral and the nuclear liquid-gas transitions. Phys. Rev. C **96**, 025205 (2017). https://doi.org/10.1103/PhysRevC.96.025205
61. J. Xu, L.W. Chen, C.M. Ko et al., Shear viscosity of neutron-rich nucleonic matter near its liquid-gas phase transition. Phys. Lett. B **727**, 244 (2013). https://doi.org/10.1016/j.physletb.2013.10.051
62. O. Savchuk, V. Vovchenko, R.V. Poberezhnyuk et al., Traces of the nuclear liquid-gas phase transition in the analytic properties of hot QCD. Phys. Rev. C **101**, 035205 (2020). https://doi.org/10.1103/PhysRevC.101.035205
63. R. Wang, Y.G. Ma, R. Wada et al., Nuclear liquid-gas phase transition with machine learning. Phys. Rev. Res. **2**, 043202 (2020). https://doi.org/10.1103/PhysRevResearch.2.043202
64. R.V. Poberezhnyuk, V. Vovchenko, A. Motornenko et al., Chemical freeze-out conditions and fluctuations of conserved charges in heavy-ion collisions within a quantum van der Waals model. Phys. Rev. C **100**, 054904 (2019). https://doi.org/10.1103/PhysRevC.100.054904
65. V. Vovchenko, M.I. Gorenstein, H. Stöecker et al., interactions in hadron resonance gas: from nuclear matter to lattice QCD. Phys. Rev. Lett. **118**, 182301 (2017). https://doi.org/10.1103/PhysRevLett.118.182301
66. R.V. Poberezhnyuk, O. Savchuk, M.I. Gorenstein et al., Higher order conserved charge fluctuations inside the mixed phase. Phys. Rev. C **103**, 024912 (2021). https://doi.org/10.1103/PhysRevC.103.024912
67. X.R. Yang, G.Y. Shao, W.B. He, Fifth- and sixth-order net baryon number fluctuations in nuclear matter at low temperature. Phys. Rev. C **109**, 014908 (2024). https://doi.org/10.1103/PhysRevC.109.014908
68. M. Bluhm, A. Kalweit, M. Nahrgang et al., Dynamics of critical fluctuations: theory - phenomenology - heavy-ion collisions. Nucl. Phys. A **1003**, 122016 (2020). https://doi.org/10.1016/j.nuclphysa.2020.122016
69. R. Bellwied, S. Borsányi, Z. Fodor et al., Fluctuations and correlations in high temperature QCD. Phys. Rev. D **92**, 114505 (2015). https://doi.org/10.1103/PhysRevD.92.114505

70. R. Wen, W.J. Fu, Correlations of conserved charges and QCD phase structure. Chin. Phys. C **45**, 044112 (2021). https://doi.org/10.1088/1674-1137/abe199
71. H.T. Ding, S. Mukherjee, H. Ohno et al., Diagonal and off-diagonal quark number susceptibilities at high temperatures. Phys. Rev. D **92**, 074043 (2015). https://doi.org/10.1103/PhysRevD.92.074043
72. S. Borsányi, Z. Fodor, J.N. Guenther et al., Higher order fluctuations and correlations of conserved charges from lattice QCD. J. High Energy Phys. **10**, 205 (2018). https://doi.org/10.1007/JHEP10(2018)205
73. R. Bellwied, S. Borsányi, Z. Fodor et al., Off-diagonal correlators of conserved charges from lattice QCD and how to relate them to experiment. Phys. Rev. D **101**, 034506 (2020). https://doi.org/10.1103/PhysRevD.101.034506
74. W.J. Fu, Y.L. Wu, Fluctuations and correlations of conserved charges near the QCD critical point. Phys. Rev. D **82**, 074013 (2010). https://doi.org/10.1103/PhysRevD.82.074013
75. A. Bhattacharyya, P. Deb, A. Lahiri et al., Correlation between conserved charges in Polyakov-Nambu-Jona-Lasinio model with multiquark interactions. Phys. Rev. D **83**, 014011 (2011). https://doi.org/10.1103/PhysRevD.83.014011
76. H.T. Ding, F. Karsch, S. Mukherjee, Thermodynamics of strong-interaction matter from lattice QCD. Int. J. Mod. Phys. E **24**, 530007 (2015). https://doi.org/10.1142/S0218301315300076
77. K. Fukushima, Hadron resonance gas and mean-field nuclear matter for baryon number fluctuations. Phys. Rev. C **91**, 044910 (2015). https://doi.org/10.1103/PhysRevC.91.044910
78. N.K. Glendenning, *COMPACT STARS, nuclear physics, particle physics, and general relativity*, 2nd edn. (Springer, New York, 2000), p.189
79. J. Cleymans, H. Oeschler, K. Redlich et al., Comparison of chemical freeze-out criteria in heavy-ion collisions. Phys. Rev. C **73**, 034905 (2006). https://doi.org/10.1103/PhysRevC.73.034905